Modeling of Neoclassical Tearing Mode Stabilization by Electron Cyclotron Heating and Current Drive in Tokamak Plasmas

Kyungjin Kim[1], Yong-Su Na[1*], Hyun-Seok Kim[1], M. Maraschek[2], E. Poli[2], J. Stober[2], H. Zohm[2], F. Felici[3], O. Sauter[3], Y.S. Park[4], L. Terzolo[5], ASDEX Upgrade team[2], and TCV Team[3]

[1]Department of Nuclear Engineering, Seoul National University, Seoul, Korea

[2]Max-Planck-Institut fuer Plasmaphysik, EURATOM Association, Garching bei München, Germany

[3]Centre de Recherches en Physiques des Plasmas, Ecole Polytechnique Fédérale de Lausanne (CRPP-EPFL), Lausanne, Switzerland

[4]Department of Applied Physics and Applied Mathematics, Columbia University, New York, USA

[5]National Fusion Research Institute, Daejeon, Korea

[*]E-mail: ysna@snu.ac.kr

Abstract.

An integrated numerical system is established to model time-dependent behavior of the neoclassical tearing mode (NTM) in a tokamak which solves the modified Rutherford equation (MRE) by coupling with plasma transport, equilibrium, heating and current drive self-consistently. The MRE is formulated by considering the electron cyclotron heating (ECH) effect as well as the electron cyclotron current drive (ECCD) effect to stabilize the NTM which is well-suited for time-dependent simulations including a predictive purpose. The integrated numerical system is applied to experiments in which NTMs are stabilized by ECCD and by ECH at ASDEX Upgrade and TCV, respectively. It is found that the simulation results catch the main experimental trend.

Keywords: **Neoclassical Tearing mode, Time-dependent simulation, the modified Rutherford equation, ECH/CD, Tokamak**

1. Introduction

As a kind of resistive MHD instabilities, the neoclassical tearing mode (NTM) is destabilized due to a localized loss of bootstrap current within a magnetic island. The NTM can significantly degrade confinement and angular momentum and even lead to plasma disruptions. Due to this potential deleterious impact on plasma confinement, suppression or avoidance of NTM is a high priority task to sustain high plasma performance in fusion experiment. Among various methods which have been proposed to date for this task, the most promising one is thought be applying electron cyclotron heating and current drive (ECH/CD) to compensate the missing bootstrap current inside the island. Since this method was introduced in FY 1997 and after pioneering experiments in ASDEX Upgrade [1], complete suppression of NTMs has been successfully achieved on many tokamaks such as ASDEX Upgrade [2], DIII-D [3-4], and JT-60U [5-6]. In parallel with experiments, numerical studies of NTM [7-12] have been performed using various numerical codes mostly with the ECH/CD effect. These numerical works focused on investigating ways for effective stabilization of the NTM such as examining the necessary EC power by solving the modified Rutherford equation (MRE) which governs the NTM behavior. In these previous works, however perfect alignment of EC to the island is assumed or modeling is done in partially self-consistent way.

An integrated numerical system is established in this work for self-consistent and time-dependent simulations of the NTM behavior in tokamak plasmas. This is eventually for the purpose of developing a feedback controller to stabilize NTMs in a tokamak. The MRE is solved by being coupled with the plasma equilibrium, transport, heating and current drive in a self-consistent way. This paper is organized as follows. In Section 2, the formulation of the MRE is described. A numerical approach is introduced in Section 3 for description of the NTM in self-consistent time-dependent simulations. As for applying the integrated numerical system to tokamak experiments, NTM stabilization experiments using ECCD and ECH in ASDEX Upgrade and TCV, respectively are described in Section 3. The results of simulations applied to these experiments are described in Section 4 and summary is given in Section 5.

2. The modified Rutherford equation (MRE) for NTM modeling

The MRE encapsulates the temporal behavior of NTM though the governing physics of the equation is not yet conclusive. The MRE estimates the growth rate of a magnetic island width to analyze the stability of NTM by taking into account the physical processes determine the growth of NTM. The general form of MRE including terms to stabilize or destabilize NTM is as follows;

$$\frac{\tau_R}{r_s^2}\frac{dw}{dt} = \Delta'_0 + \Delta'_{BS} + \Delta'_{pol} + \Delta'_{GGJ} + \Delta'_{EC} + \cdots$$

where w is the island width, τ_R the resistive time, and r_s the radius at the resonant surface. The terms on the right-hand side, Δ'_0, Δ'_{BS}, Δ'_{pol}, Δ'_{GGJ}, and Δ'_{EC} represent effects of the equilibrium current profile, the perturbed bootstrap current, the ion polarization current, the equilibrium pressure gradient and the favorable curvature in a toroidal geometry (so-called as the Glasser–Green–Johnson (GGJ) effect [13]), and the ECH/CD,

respectively. There could be other mechanisms affecting NTM such as the effect of the fast particles, the error field, the plasma rotation, the nonlinear mode coupling, and micro-instabilities which need to be taken into account to make the NTM theory complete. According to physical assumptions adopted in the analysis, each term in the MRE can come up with different forms though they represent the same physics.

As MRE can be formulated in several shapes, we adopt one which satisfies the following requirements suitable for self-consistent time-dependent simulations. First of all, it should solve the time evolution of the NTM with assumptions as low as possible with minimum number of free parameters well-suited for predictive simulations. Secondly, it should be directly coupled with a transport solver for self-consistent simulations. Thirdly, it should include both ECCD and ECH effects. Additionally, it should predict the island width fast enough relevant to design a feedback controller.

A MRE formulation [14] which satisfies the above requirements is employed in this work for modelling of the NTM behaviour. We newly added a term dealing with the contribution of the ECH to the MRE [15, 16] so that it is written as following;

$$\frac{\tau_R}{r_s}\frac{dw}{dt} = \Delta_0^{'} r_s + \delta\Delta^{'} r_s + a_2 \frac{j_{bs}}{j_{\parallel}}\frac{L_q}{w}\left[1 - \frac{w_{marg}^2}{3w^2} - K_1\frac{j_{ec}}{j_{bs}} - \tilde{\alpha}_H \frac{w}{w_{dep}}\frac{P_{ec}\eta_H}{I_{ec}}\right]$$

where a_2 is a shaping and finite aspect ratio factor, $j_{\parallel}$ is the equilibrium current density parallel to the magnetic field, j_{bs} is the local bootstrap current density, and j_{ec} is the peak current density driven by EC injection. The magnetic shear length, L_q is defined as $L_q = q/(dq/dr)$ and the marginal island width, w_{marg} is the characteristic island width at the maximum growth rate. K_1 represents the effectiveness of the external current drive for compensating the missing bootstrap current, and $\tilde{\alpha}_H$ is the geometrical function representing the inductive current due to temperature perturbations inside the island by ECH. η_H is defined as the inductive current generation efficiency converted from the injected power, P_{ec}. w_{dep} is the power deposition width of EC.

The first term of right-hand side, $\Delta_0' r_s$, implies the conventional tearing mode stability. In this formulation, $\Delta_0' r_s$ is assumed to be $\Delta_0' r_s \approx -m$ as a value between the marginal classical stability ($\Delta_0' r_s \approx 0$) and strong stability ($\Delta_0' r_s \approx -2m$) [17] for the (m,n) NTM characterized by a large bootstrap current and with a stable current profile as used in [18-20]. Note that the (m,n) notation describes the poloidal and the toroidal mode number, respectively. The second term, $\delta\Delta' r_s$ determines the tearing mode stability enhancement by EC considering the fact that the external current drive can make Δ_0' more negative due to change the total local equilibrium current density $j_{\parallel}$. If the EC is injected with a modulation with a duty cycle τ, the change in Δ' is defined using Westerhof's model with no-island assumption [21] as $\delta\Delta' r_s \approx -\frac{5\pi^{3/2}}{32} a_2 \frac{L_q}{\delta_{ec}} F(\tilde{e}) \frac{j_{ec}}{j_{\parallel}} \tau$, where δ_{ec} is the full width half-maximum (FWHM) of the EC deposition width and $F(\tilde{e})$ is the function for the misalignment effect between the EC deposition and the island, $F(\tilde{e}) = 1 - 2.43\tilde{e} + 1.40\tilde{e}^2 - 0.23\tilde{e}^3$, where $\tilde{e} = |r - r_s|/\delta_{ec}$. The second term is determined when $0 \le \tilde{e} \le 2.25$. The third term describes the destabilization effect from the perturbed bootstrap currents. The geometric coefficient a_2 can be inferred from the saturated island width (w_{sat}) where $dw/dt \approx 0$ at $w = w_{\mathrm{sat}}$. The forth term yields the stabilization effect from small island and the polarization threshold. In the scaling for (3,2) NTM metastability threshold against normalized poloidal ion Larmor radius, it is consistent with the marginal island width about twice the ion

banana width [19] as $w_{marg} \approx 2\epsilon^{1/2}\rho_{\theta i}$ where ϵ is the local inverse aspect ratio and $\rho_{\theta i} = \sqrt{2m_i k_B T_i / e^2 B_\theta^2}$ is the local poloidal ion gyroradius. This assumption is also applied to the (2,1) NTM. The fifth term exhibits the stabilization effect of replacing bootstrap current by ECCD. The effectiveness parameter K_1, determined by a matrix depending on the ECCD inside the island, is calculated using the relative narrowness and misalignment of ECCD [19, 22]. The last term of right hand side describes the stabilization effect of ECH contribution. The details concerning η_H and $\tilde{\alpha}_H$ can be found in [15, 16, 23]. It is noteworthy that the GGJ effect can be neglected in this MRE for large aspect ratio plasmas [24].

As defined above, this MRE formulation has a great advantage in predictive simulations for designing controller since all the parameter and coefficients in this MRE can be determined self-consistently in time-dependent simulations. Although some "ad-hoc" assumptions cannot be avoided, the number of free parameters is minimized for this purpose.

3. The numerical approach

3.1. The integrated numerical system for self-consistent NTM simulations

In order to describe the time evolution of the NTM behavior self-consistently, plasma equilibrium, transport, and H/CD need to be solved together with the MRE. As illustrated in figure 1, the plasma parameters and the island of NTM are closely linked each other through the plasma equilibrium, transport, and H/CD. The electron temperature profile and the current density profile are affected by ECH/CD that is used for controlling the NTM. On the other hand, the deposition of ECH/CD and the location of island are varying in time in response to evolution of the plasma equilibrium which is strongly involved with the current density profile. The heat diffusivities are modified at the island location over the island width so that the NTM affects plasma transport. To take all this into account, an integrated numerical system is required which incorporates the plasma equilibrium, the transport, the H/CD, and the MRE.

As for the transport solver, the core of the integrated system, ASTRA (Automated System for TRansport Analysis) [25] is employed, which solves time-dependent 1D transport equations for particle, heat, and current on each magnetic flux surface. It is coupled with equilibrium solvers such as ESC (Equilibrium and Stability Code) [26] for fixed boundary plasma equilibria or the 3-moment equilibrium solver for up-down symmetric configurations for dealing with a realistic tokamak geometry. The ASTRA code is relatively fast and easy to implement various modules, functions, and subroutines to it. A number of other modules for auxiliary H/CD are incorporated in the ASTRA code. For example, the NBI (Neutral Beam Injection) package [27] is embedded in ASTRA for calculation of the NBI H/CD and TORAY-GA (TOkamak ECH/CD RAY-tracing code) [28] for calculation of ECH/CD. To simulate the ray pattern of an actual antenna, the ray pattern generator is used as to make the rays consistent with a Gaussian distribution. The relativistic wave absorption along the ray path is computed in TORAY-GA using the Matsuda-Hu damping model that solves the dispersion relation in the cold or the warm plasma approximation in the vicinity of desired harmonic. The ECCD is computed using a formulation by Y. R. Lin-Liu [29] using the numerical solution for the Spitzer-Harm problem including the

trapped particles, electron-ion collisions, and poloidal variation of the collision operator. A numerical module (the MRE solver) is constructed to solve the MRE, which is merged into the numerical integrated system to communicate with ASTRA, equilibrium solvers, and H/CD modules. An overview of the structure of the integrated numerical system for NTM modeling is presented in figure 2.

3.2. Approach to describe NTM in time-dependent simulations

The integrated numerical system is designed to deal with two types of simulations. One is for interpretative and the other is for predictive simulations. Note that we focus on the interpretative simulation in this work for benchmarking of our methodology before applying to predictive simulations. The predictive simulations can be used for predicting the NTM behavior and simulating feedback control of NTM in a tokamak.

Interpretative simulation

The time evolution of the island is calculated by using experimental data in interpretative simulations. Ion and electron temperature profiles, electron density profiles, the effective ion charge Z_{eff}, the radiation power, and the plasma configurations are provided as a time-varying input to the integrated numerical system. Then, the variables in MRE such as j_{bs}, $j_{\parallel}$, L_q, r_s, and τ_R are calculated by ASTRA. The geometric coefficient a_2 is inferred from the saturated island width (w_{sat}) observed by the experiment. The a_2 is calculated when the NTM occurs and kept as a constant afterwards in the simulation. All these variables of MRE are passed to the MRE solver so that the island width can be calculated by $w_{new} = w_{old} + (dw/dt)\times\Delta t_{sim}$ and updated at every simulation time step.

The procedure of computation is following (marked in black and red in figure 3):

1. Importing the initial data from the experiment
2. Solving MHD equilibrium (ESC)
3. Calculating the driven current (NBI module, TORAY-GA) and the bootstrap current (ASTRA)
4. Solving current diffusion using the kinetic profiles (ASTRA): Calculating the Ohmic current density and the total current density ($j_{\parallel}$, $j_{\parallel} = j_{OH}+j_{CD}+j_{bs}$)
5. Solving MRE by importing information of j_{bs}, $j_{\parallel}$, L_q, r_s, and τ_R from ASTRA (MRE solver)
6. Importing kinetic profiles of the next time step from the experiment and loading the calculated total current density profile for the next time step simulation
7. Go back to step 2 and repeat

Predictive simulation

The time evolution of the island is calculated by using mostly self-simulated data in predictive simulations. Ion and electron temperature profiles and electron density profiles can be calculated by theory-based transport models such as the Weiland model [30] and the GLF model [31] for anomalous transport and the Angioni-Sauter model [32] and the Galeev-Sagdeev model [33] for neoclassical transport. The effective ion charge Z_{eff} can be prescribed and the radiation power can be calculated by including the Bremsstrahlung, the cyclotron, and the line radiation. The plasma configurations are prescribed as a time-varying input to the integrated numerical

system. Then, the variables in MRE such as $j_{bs}, j_{\parallel}, L_q, r_s$, and τ_R are calculated by ASTRA. The a_2 is calculated when the NTM occurs using the saturated island width determined by the ISLAND module [34] and kept as a constant afterwards in the simulation. All these variables of MRE are passed to the MRE solver so that the island width can be calculated and updated at every time step. Flattening of kinetic profiles inside the magnetic island is considered in predictive simulations by increasing diffusivities deliberately in the electron and the ion channel so that the NTM effects are taken into account in transport simulations in a self-consistent way: $\chi_{i,e} \approx c_\chi\left(\chi_{i,e}^{Neoclassical} + \chi_{i,e}^{Anomalous}\right)$ inside the island, otherwise, $\chi_{i,e} = \chi_{i,e}^{Neoclassical} + \chi_{i,e}^{Anomalous}$ where $\chi_{i,e}^{Neoclassical}$ and $\chi_{i,e}^{Anomalous}$ are neoclassical and anomalous heat diffusivity, respectively for the ion and the electron (a similar methodology appears in [35]).

The procedure of computation is following (marked in black and blue in figure 3):

1. Importing the prescribed initial kinetic and current density profile
2. Solving MHD equilibrium (ESC)
3. Calculating the driven current (NBI module, TORAY-GA) and the bootstrap current (ASTRA)
4. Solving current diffusion using the kinetic profiles (ASTRA): Calculating the Ohmic current density and the total current density ($j_{\parallel}=j_{OH}+j_{CD}+j_{bs}$)
5. Solving MRE by importing information of $j_{bs}, j_{\parallel}, L_q, r_s$, and τ_R from ASTRA (MRE solver)
6. Modifying diffusivities inside the island (ASTRA)
7. Solving transport (ASTRA): Calculating temperature and density profiles
8. Loading the calculated total current density, temperature and density profile for the next time step simulation
9. Go back to step 2 and repeat

4. Benchmark and applications of the NTM modeling

The experiments for NTM stabilization using ECCD and ECH are chosen from ASDEX Upgrade and from TCV, respectively to benchmark our numerical approach. Table 1 summarizes the input data and the models used in interpretative simulations for each device. As input for the simulations, profiles of the ion and the electron temperature, the electron density, and the toroidal rotation are taken from experiments. In case of ASDEX Upgrade, the toroidal rotation is estimated from the other pulse 17870 [37] and the poloidal rotation is assumed to be neoclassical. In case of TCV, both the toroidal and the poloidal rotation can be negligible compared with ASDEX Upgrade because they are Ohmic discharges. The effective ion charge Z_{eff} is assumed to be constant during the simulation. The radiation power is calculated in the simulations by including the Bremsstrahlung, the cyclotron and the line radiation from carbon.

4.1. ASDEX Upgrade discharges [38, 39]

Two shots in ASDEX Upgrade, pulse 21133 and 25845, are selected to evaluate the capability of reproducing the NTM behavior using the integrated numerical system described in section 3. Figure 4 represents the time evolution of each discharge. The plasma current and the magnetic field are 0.801 MA and ~2 T, respectively

for pulse 21133 and 1.002 MA and 2.524 T, respectively for pulse 25845. Both discharges are designed to suppress the (3,2) NTM using co-ECCD aligned to the island location, but their specific methods to vary the localization of the EC wave absorption are different. In pulse 21133, the magnetic field is ramped up from 2 T to 2.3 T to change the EC wave deposition relative to the NTM by moving the resonance surface outward. In pulse 25845, on the other hand, the poloidal and the toroidal launcher angle are varied via a movable mirror to adjust the EC wave deposition by using the feed-forward control. Recently, a fast movable launcher was installed in ASDEX Upgrade, which can move at a speed of 10 ° in 100 ms during a pulse [38]. The varying parameter in experiments, the magnetic field B_T for pulse 21133 and the poloidal angle of EC launcher θ for pulse 25845, and the corresponding response of the amplitude of (3,2) NTM are also presented in figure 4. In both these cases, β_N is observed to drop significantly after occurrence of the NTM and to recover slightly after stabilization of the NTM.

The simulations start at 1.0 s in order to adjust the q-profile when the plasma current almost reaches the flat-top phase. The time step for simulations is adjusted between 0.02 ms and 1.0 ms. A seed island for NTM is forced to appear in simulations at 1.75 s with 0.06 m of width and at 1.7 s with 0.02 m of width for pulse 21133 and 25845, respectively. The a_2 is calculated as 6.27 and 5.36 for pulse 21133 and 25845, respectively at the same time of the island onset. For both cases, the experimental saturated island width, 0.06 m is used. As shown in figure 5, the time evolution of the island width follows the trend of the experiment until the rapid stabilization phase. For pulse 21133, the simulated island increases instantly around 3.0 s so that the island is not suppressed but survived for slightly longer time than the experiment. For pulse 25845, the simulated island decreases continuously around 2.7 s so that the island is suppressed slightly faster than the experiment. It is noteworthy that the simulations are highly sensitive to the q-profile since the local parameters such as L_q and $j_{||}$ in MRE as well as the island location are influenced by the q-profile.

4.2. TCV discharges [40]

The NTM experiments on TCV (pulse 40539 and 40543) showed that the efficiency of the NTM suppression is dominated by the ECH inside the island. This is consistent with the relatively low current drive efficiency under the conditions of the TCV experiments and the far off-axis of the $q = 2$ position. Two discharges are almost identical except the applied EC power to suppress the (2,1) NTM. Figure 6 represents the time evolution of main plasma parameters and variables. The plasma current and the magnetic field are 0.2 MA and 1.44 T, respectively, same to both discharges. In pulse 40539, ~0.21 MW of EC power is applied to the $q = 2$ surface from 0.9 s. On the other hand, in pulse 40543, ~0.57 MW is applied from 0.9 s to 1.1 s and ~0.21 MW after 1.1 s. In both discharges, β_{pol} and β_{tor} are observed to drop significantly after occurrence of the NTM. Note that the amplitude of the MHD signal in figure 6 represents not the amplitude of the mode but the existence of the mode.

The simulations to reproduce the discharges at TCV start at 0.2 s with initial plasma profiles from the experiment. The time step for simulations is adjusted between 0.01 ms and 1.0 ms. The equilibria for these shots are reconstructed using the integrated numerical system described in section 3 employing the 3-moment equilibrium solver, which can handle double null (DN) configurations being used in these experiments. A seed

island is forced to appear with $3.5\,cm$ at $0.3\,s$ in the simulations for both cases. At the same time step, the calculated a_2 is 17.37 using the experimental saturated island width of $\sim 5.5\,cm$. The results are shown in figure 7. The island growth rate slightly changes according to the plasma condition but close to zero prior to the EC injection at 0.9 s. The saturated island width decreases rapidly after the EC injection because the EC power is well-aligned with the position of the (2,1) NTM. As seen in figure 7 and 8, it is found that the EC power can affect the growth rate of the island significantly. Because of a relatively small EC power, the island is not suppressed completely, however saturated again but with a reduced saturated island size about $3.5\,cm$ in pulse 40539 while the island is fully suppressed in pulse 40543. As shown in figure 8, the ECH term plays a dominant role on stabilizing the NTM.

5. Summary

An integrated numerical system is developed to simulate the NTM stabilization by ECH and ECCD in a tokamak. It solves the modified Rutherford equation (MRE) by coupling plasma transport, equilibrium, heating and current drive self-consistently. A MRE suitable for self-consistent simulation is formulated by considering the ECH as well as the ECCD effect. The integrated numerical system is benchmarked against experiments in ASDEX Upgrade and in TCV where the NTMs are stabilized by ECCD and by ECH, respectively. The main experimental trends are well reproduced by the integrated numerical system. The integrated numerical system is envisaged to contribute to design and optimize a NTM controller using ECH/CD in tokamaks.

Acknowledgements

The authors would like to thank Doohyun Kim for useful discussions and supports. The authors would also like to acknowledge the ASDEX and TCV team for their experimental support and for useful discussions.

This work was supported by the National Research Foundation of Korea (NRF) grant funded by the Korea government (MSIP) (No. 20080061900) and by R&D Program through the National Fusion Research Institute of Korea (NFRI) funded by the Government funds.

References

[1] H. Zohm, et al., *Nucl. Fusion* **39**, 577 (1999)

[2] G. Gantenbein, et al., *Phys. Rev. Lett.* **85**, 1242 (2000)

[3] R. J. La Haye, et al., *Phys. Plasmas* **9**, 2051 (2002)

[4] C. C. Petty, et al., *Nucl. Fusion* **44**, 243 (2004)

[5] A. Isayama, et al., *Nucl. Fusion* **43**, 1272 (2003)
[6] A. Isayama, et al., *Nucl. Fusion* **47**, 773 (2007)
[7] A. M. Popov, et al., *Phys. Plasmas* **9**, 4205 (2002)
[8] N. Hayashi, et al., *Nucl. Fusion* **44**, 477 (2004)
[9] K. Nagasaki, et al., *Nucl. Fusion* **45**, 1608 (2005)
[10] A. Isayama and the JT-60 Team, *Plasma science and Technology* **8**, 36 (2006)
[11] Y. S. Park, Ph.D. Dissertation, Seoul National University (2008)
[12] G. Falchetto, et al., *Nucl. Fusion* **54**, 043018 (2014)
[13] H. Lütjens and J. F. Luciani, *Phys. Plasmas* **9**, 4387 (2002)
[14] R. J. La Haye, *Phys. Plasmas* **13**, 055501 (2006)
[15] D. De Lazzari and E. Westerhof, *Nucl. Fusion* **49**, 075002 (2009)
[16] D. De Lazzari and E. Westerhof, *Nucl. Fusion* **50**, 079801 (2010)
[17] D. P. Brennan, et al., *Phys. Plasmas* **9**, 2998 (2002)
[18] O. Sauter, et al., *Plasma Phys. Control. Fusion* **44**, 1999 (2002)
[19] R. J. La Haye, et al., *Nucl. Fusion* **46**, 451 (2006)
[20] Y. S. Park, et al., *J. Korean Phys. Society* **53**, 1923 (2008)
[21] E. Westerhof, *Nucl. Fusion* **30**, 1143 (1990).
[22] F. W. Perkins, et al., *Proc. 24th EPS Conf. on Controlled Fusion and Plasma Physics (Berchtesgaden, Germany, 1997)* P.1017 (1997)
[23] B. Ayten, et al., *Nucl. Fusion* **51**, 043007 (2011)
[24] R. J. La Haye, et al., *Phys. Plasmas* **19**, 062506 (2012)
[25] G. Pereverzev, "Automated System for Transport Analysis", MPI fur PP Report ZB:IPP 5-98 (2002)
[26] L. E. Zakharov, et al., *Phys. Plasmas* **6**, 4693 (1999)
[27] A. Polevoi, et al., JAERI-Data/Code 97-014 (1997)
[28] K. Matsuda, *IEEE Trans. Plasma Sci.* **17**, 6 (1989)
[29] Y. R. Lin-Liu, et al., *Phys. Plasmas* **10**, 4064 (2003)
[30] J. Weiland, et al., *Nucl. Fusion* **29**, 1810 (1989)
[31] R. E. Waltz *et al*., *Phys. Plasmas* **4**, 2482 (1997)
[32] C. Angioni and O. Sauter, *Phys. Plasmas* **7**, 1224 (2000)
[33] A. A. Galeev and R. Z. Sagdeev, *Voprosy Teorii Plasmy* **7**, 210 (1973)
[34] F. D. Halpern, et al., *J. Plasma Physics* **72**, 1153 (2006)
[35] G. Turri, et al., *Proc. 22nd IAEA Fusion Energy Conference* (Geneva, Switzerland, 2008), EX/P3-6 (2008)
[36] O. Sauter, et al., *Phys. Plasmas* **6**, 2834 (1999)
[37] Yong-Su Na, et al., *Nucl. Fusion* **46**, 232 (2006)
[38] M. Reich, et al., *Fusion Sci. Technol.* **61**, 309 (2012)
[39] J. Stober, et al., *Proc. 16th Joint Workshop on Electron Cyclotron Emission and Electron Cyclotron Resonance Heating (Sanya, Chana, 2010)* (2010)
[40] O. Sauter, et al., *Proc. 23th IAEA Fusion Energy Conference (Daejeon, Korea, 2010)*, EXS/P2-17 (2010)

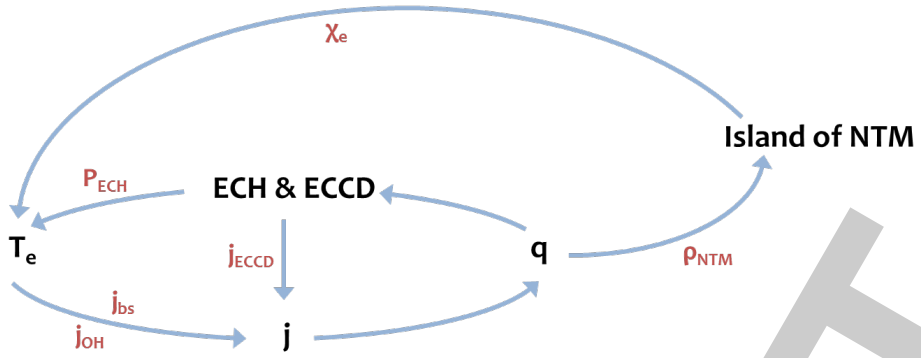

Figure 1 The close relation between the island of NTM (position ρ_{NTM} and width w) and the plasma parameters (temperature T, current density j, safety factor q, and heat diffusivity χ_e).

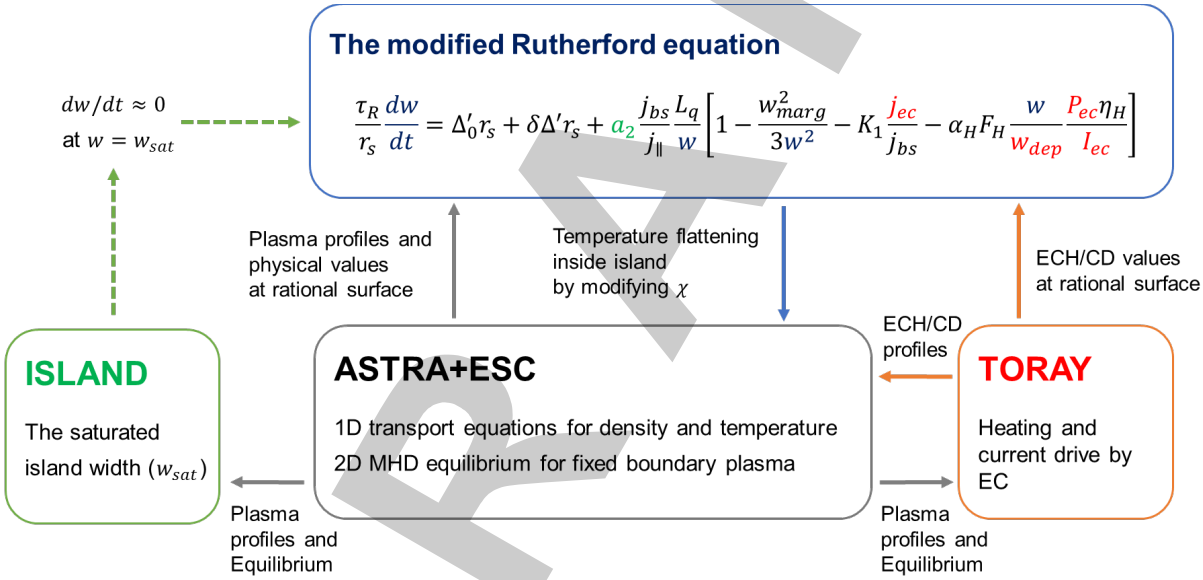

Figure 2 Overview of the structure of the integrated numerical system for NTM modeling.

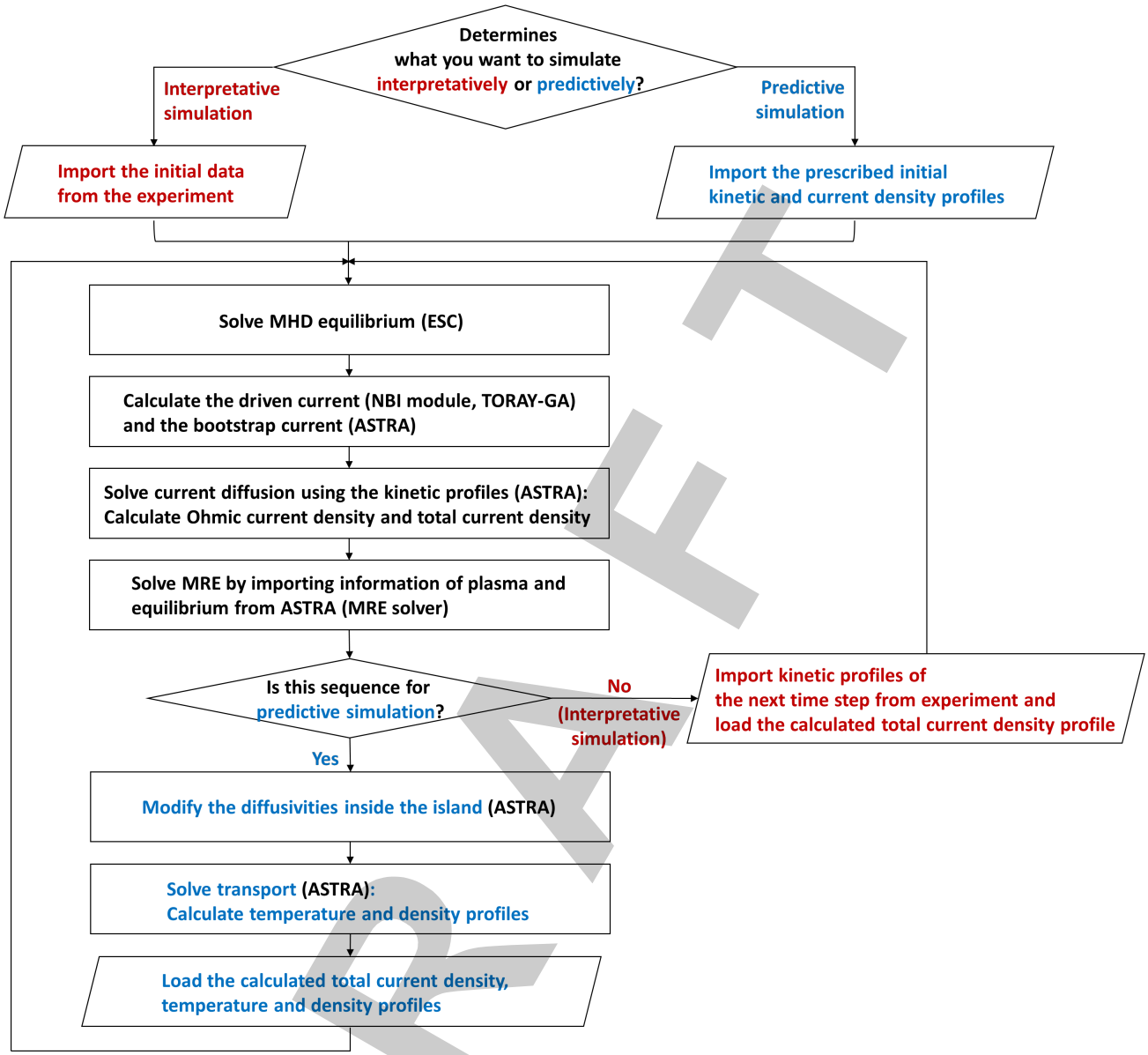

Figure 3 Flow chart of the procedure of computation; for interpretative simulations (red) and for predictive simulations (blue).

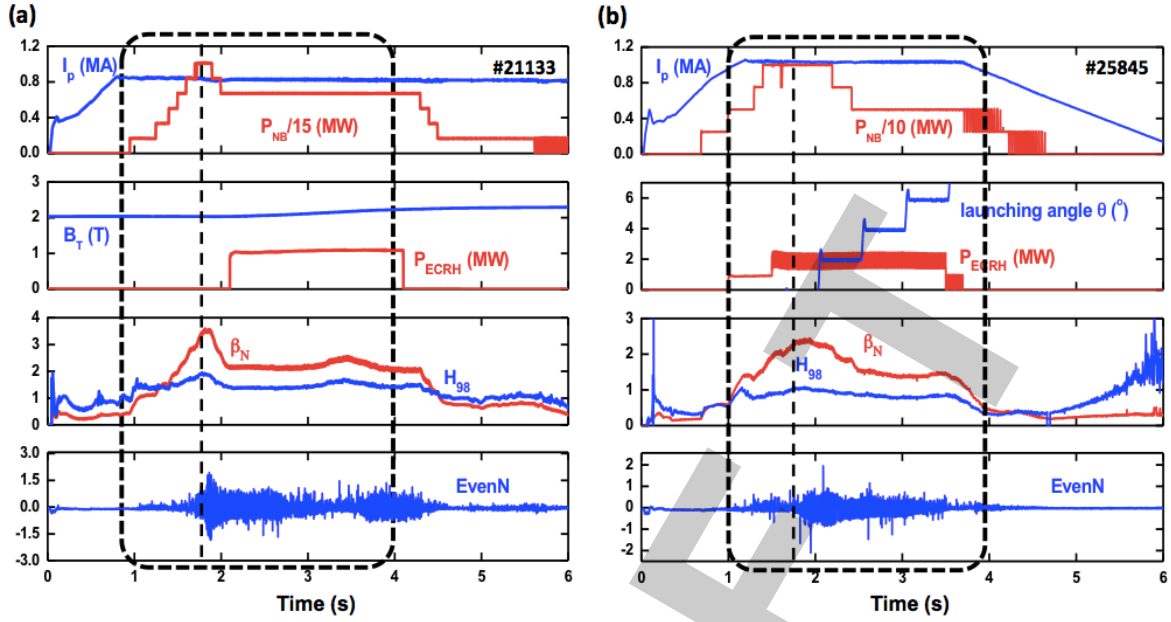

Figure 4 The time traces of plasma current I_p, NB heating power P_{NB}, varying parameter for aligning the EC deposition to the island position (magnetic field B_T and poloidal angle of EC launcher θ for pulse 21133 and pulse 25845, respectively), EC heating power P_{ECRH}, normalized beta β_N, confinement enhancement factor $H_{98(y,2)}$, the amplitude of Mirnov signals for even toroidal mode numbers dominated by the (3,2); for a NTM stabilization experiment by B_T scan (pulse 21133) (a) and by launching angle scan (pulse 25845) (b) in ASDEX Upgrade.

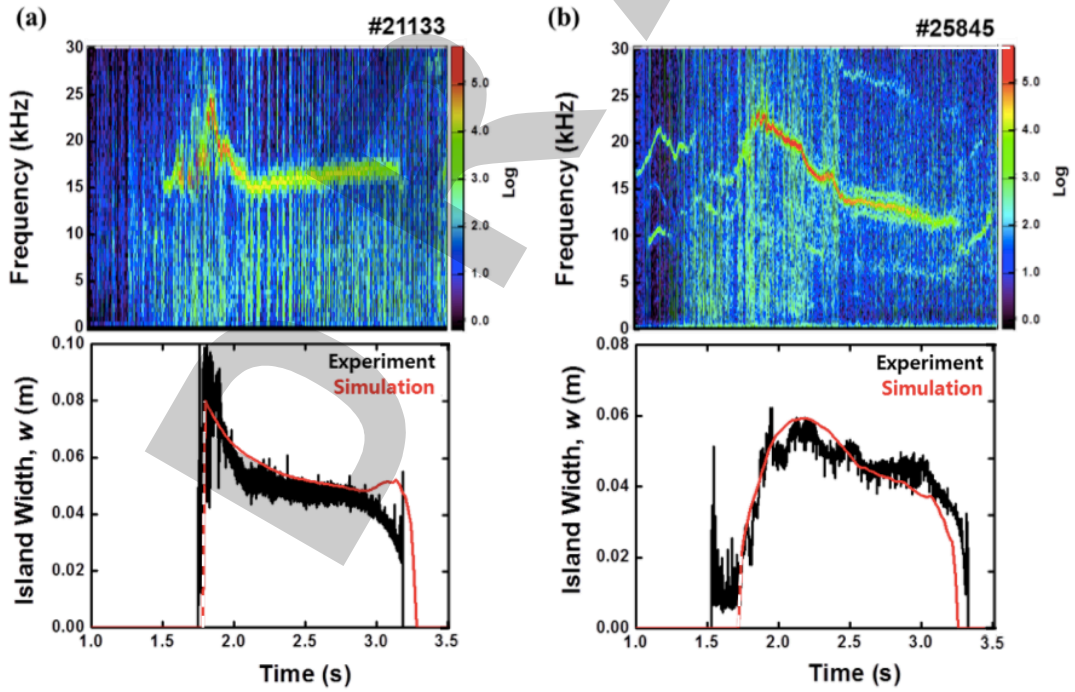

Figure 5 Time trances of fast Fourier transform (FFT) frequency spectrum of magnetic pickup coil signals (top) and comparison of time evolution of the island width of (3,2) NTM between the experiment and the simulation (bottom) for pulse 21133 (a) and for pulse 25845 (b).

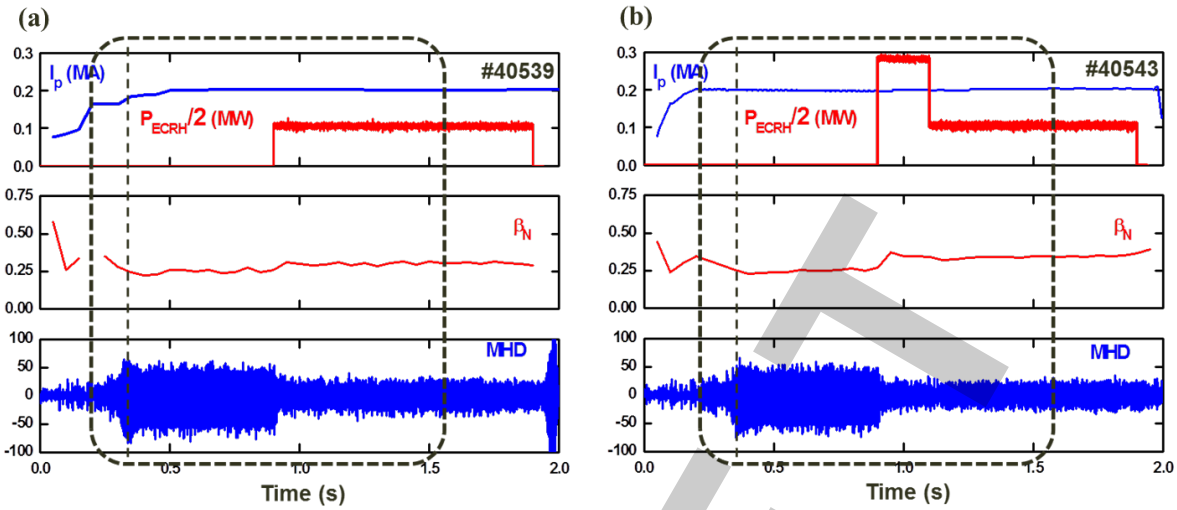

Figure 6 The time traces of plasma current I_p, EC heating power P_{ECRH}, normalized beta β_N, and the amplitude of MHD signals for (2,1) NTM; (a) partial stabilization experiment of NTM (pulse 40539) and (b) full stabilization experiment of NTM (pulse 40543) in TCV.

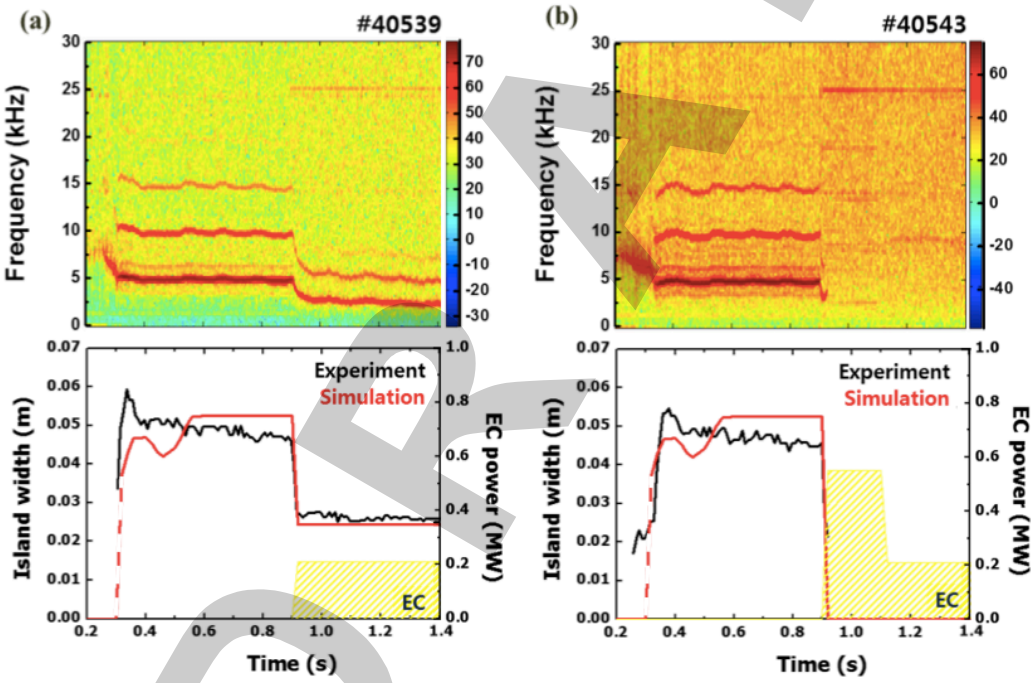

Figure 7 Time traces of FFT frequency spectrum of magnetic pickup coil signal (top) and comparison of time evolution of the island width of (2,1) NTM between the experiment at TCV and the simulation (bottom) for pulse 40539 (a) and for pulse 40543 (b).

$$\frac{\tau_R}{r_s}\frac{dw}{dt} = \Delta'_0 r_s + \delta\Delta' r_s + a_2 \frac{j_{bs}}{j_{||}}\frac{L_q}{w}\left[1 - \frac{w^2_{marg}}{3w^2}\right] - K_1 \frac{j_{ec}}{j_{bs}} - \alpha_H F_H \frac{w}{w_{dep}}\frac{P_{ec}\eta_H}{I_{ec}}$$

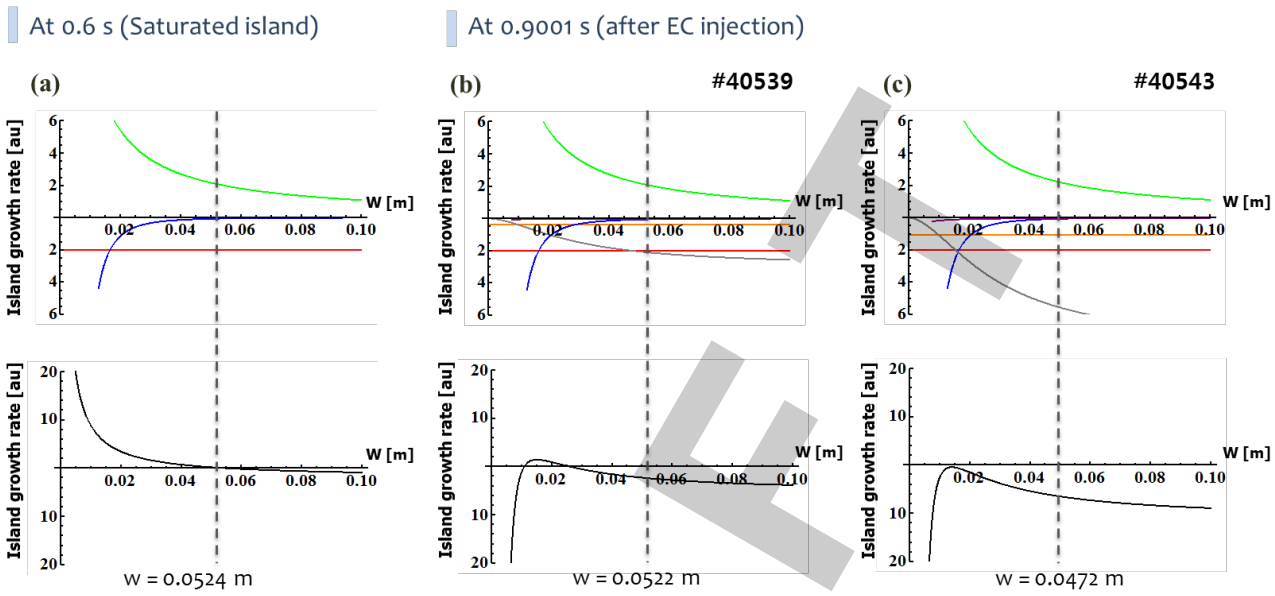

Figure 8 The (2,1) NTM stability (black) in TCV. The contribution of each term in MRE; the conventional tearing stability (red), the perturbed bootstrap current (green), the small island and polarization threshold (blue), the ECCD (orange, purple) and the ECRH (gray), which depends on the island width (gray dashed vertical line). at t = 0.6 s for both discharges (a), at t = 0.9 s for pulse 40539 (b), and at t = 0.9 s for pulse 40543 (c).

	ASDEX Upgrade	**TCV**
n_e, $T_{i,e}$	Experimental	
P_{rad}	Bremmstrahlung, Cyclotron, Line (Carbon)	
v_{tor}	Estimated (AUG, pulse 17870)	-
v_{pol}	neoclassical	-
Z_{eff}	2.0	1.5
Initial q	Experimental	
Bootstrap current	Sauter's formula [18, 36]	

Table 1 The input data and models used in interpretative simulations on ASDEX Upgrade and TCV